Chemical Nonequilibrium Effects on Flowfields for Aeroassisted Orbital Transfer Vehicles

Judy L. Shinn* and Jim J. Jones†
NASA Langley Research Center, Hampton, Virginia

Acceptable altitude and velocity ranges for the perigee of aeroassited orbital transfer venicles (AOTV) have been determined for various values of the ballistic coefficient and lift-to-drag ratio. The chemical nonequilibrium effect on the flowfield of a simple but representatively high-drag, blunt configuration was investigated for these perigee conditions, ranging 73-90 km in altitude and 8-9.3 km/s in velocity. The analysis was performed using a two-dimensional viscous shock-layer code that had previously demonstrated good success in predicting nonequilibrium heating on the Space Shuttle. The results indicate lower ratio of nonequilibrium/equilibrium heating for the present AOTV perigee conditions than for the Shuttle flight conditions, due to higher velocity. The trend for the degree of nonequilibrium with the effect of varying wall catalycity and configuration was determined over the altitude range. Some implications for future design consideration are indicated.

Nomenclature

C_i = mass fraction of species i, ρ_i/ρ
C_p = frozen specific heat of mixture, $\sum_i C_i C_{p,i}$
h_i = enthalpy of species i, h_i^*/U_∞^{*2}
k_w^* = surface catalytic recombination rate
K = thermal conductivity of mixture, $K^*/\mu_{\text{ref}}^* C_{p,\infty}^*$
M_i^* = molecular weight of species i
n = coordinate measured normal to the body, n^*/R_N^*
N_s = number of reacting species
N_{Le} = Lewis number, $N_{Le} = \rho^* D_{ij}^* C_p^*/K^*$
N_{Pr} = Prandtl number, $N_{Pr} = \mu^* C_p^*/K^*$
q_w = wall heat-transfer rate, $q_w^*/(\rho_\infty^* U_\infty^{*3})$
R_N^* = nose radius
s = coordinate measured along the body surface, s^*/R_N^*
T = temperature, T^*/T_{ref}^*
T_{ref}^* = reference temperature, $U_\infty^{*2}/C_{p\infty}^*$
u = velocity component tangent to body surface, u^*/U_∞^*
U_∞^* = freestream velocity
γ_i = catalytic recombination coefficient
ϵ = Reynolds number parameter, $\sqrt{\mu_{\text{ref}}^*/\rho_\infty^* U_\infty^* R_N^*}$
μ = viscosity of mixture, μ^*/μ_{ref}^*
μ_{ref} = reference viscosity, $\mu^*(T_{\text{ref}}^*)$
ρ = density of mixture, ρ^*/ρ_∞^*

Superscripts

(*) = dimensional quantities

Subscripts

i,j = ith and jth species
ref = reference value
w = wall value
∞ = freestream value

Abbreviations

ECW = equilibrium (or fully) catalytic wall
EQ = equilibrium
NCW = noncatalytic wall
NEQ = nonequilibrium

Introduction

VARIOUS studies have shown that a considerable saving in fuel, and therefore an increase in payload, is possible if an orbital transfer vehicle (OTV) uses the Earth's atmosphere to reduce velocity in returning to low Earth orbit from a higher energy orbit. It is possible also to alter the inclination of the orbit during this maneuver. The history of this concept is reviewed in Ref. 1. This use of the atmosphere not for entry, but to modulate the vehicle orbit, is currently referred to as aeroassist. The aeroassisted entry-exit maneuver must necessarily be performed at an altitude high enough to prevent the vehicle from being captured in the atmosphere and making a complete entry, but the altitude must be low enough to allow sufficient aerodynamic forces to accomplish the orbit modulation. Depending on the vehicle's lift-to-drag ratio (L/D) and ballistic coefficient ($\beta = M/C_D A$), the altitude of this perigee varies. For example, the aeromaneuvering orbit-to-orbit Shuttle (AMOOS),[1-4] with its relatively low L/D and relatively high β, was required to descend deep into the atmosphere to an altitude of 50 km or so to achieve the aeroassisted maneuver. Hence, an ablative heat shield was required for AMOOS. On the other hand, the most recently studied aeroassisted OTV concepts, such as the lifting brake[1,5] and the inflatable ballute[1,6,7] will permit the use of relatively low-temperature material because, with their low L/D and low β, the aerobraking maneuver can be carried out at a higher altitude of approximately 80 km range.

Flight at entry speeds in this altitude range is known to be characterized by nonequilibrium flow in the shock layer. Reference 8, for instance, shows that the Shuttle flowfield through this altitude range is quite far from that predicted by assuming chemical equilibrium. When a nonequilibrium, dissociatively reacting viscous shock-layer code was adapted to the Shuttle surface catalycity, the predicted convective heating rate was in good agreement with the STS-2 flight data.[8] In addition, the results[8] revealed that the heating reduction due to the use of the relatively noncatalytic tiles was quite significant, by as much as 50% for the high-altitude

Presented as Paper 83-0214 at the AIAA 21st Aerospace Sciences Meeting, Reno, Nev., Jan. 10-13, 1983; received March 7, 1983; revision received May 7, 1984. This paper is declared a work of the U.S. Government and therefore is in the public domain.

*Research Engineer, Aerothermodynamics Branch, Space Systems Division. Member AIAA.

†Head, Aerothermodynamics Branch, Space Systems Division. Member AIAA.

range. Although the configuration for a future OTV has not been determined yet, a parametric study for heating reduction due to nonequilibrium chemistry is expected to be beneficial to the OTV design studies.[9]

The present investigation uses the same nonequilibrium, as well as equilibrium, viscous shock-layer analysis employed in Ref. 8 for the aeroassisted OTV (AOTV) perigee conditions. To provide a range of condition for the analysis, a family of trajectories near perigee was generated for a range of values of L/D and β. Since the intent of this study was not to evaluate a specific OTV configuration, but to examine the nonequilibrium flowfield and surface effect for a representatively blunt configuration, a 45 deg half-angle hyperboloid with 2.5 m nose radius was chosen for the flowfield analysis. Comparison between calculated results from equilibrium and nonequilibrium chemistry was made for the convective heating distribution and shock-layer profiles. For the nonequilibrium chemistry, the surface heating reduction was examined by varying the surface catalycity across the altitude range. The effect of varying half-angle and nose radius on nonequilibrium heating reduction was also examined.

Analysis

Governing Equations and Boundary Conditions

The viscous shock-layer equations are obtained from the steady-state Navier-Stokes equations by keeping terms up to second order in the inverse square root of the Reynolds number ϵ.[10] Consequently, the viscous shock-layer solution, which uses one set of equations for both the inviscid and viscous regions, is superior to the conventional inviscid plus boundary-layer solution in that no approximate procedure is needed to account for entropy-layer swallowing and viscous-inviscid interaction. The viscous shock-layer equations for both equilibrium and nonequilibrium multicomponent gas mixture was developed in Ref. 11 and used in Ref. 8 without mass injection. In the present study, the same equations for a blunt axisymmetric body at zero angle of attack reported in Ref. 8 are used and, therefore, not repeated here.

The boundary conditions at the shock are calculated by using the Rankine-Hugoniot relations. At the wall, the no-slip and no-temperature-jump boundary conditions are used. For the nonequilibrium flow, the wall species concentration is dictated by the catalytic recombination rate k_w^* in the following expression:

$$\frac{\partial C_i}{\partial n} - \left(\frac{k_{w,i}\rho N_{Pr}}{N_{Le}\mu\epsilon^2}\right)C_i = 0 \tag{1}$$

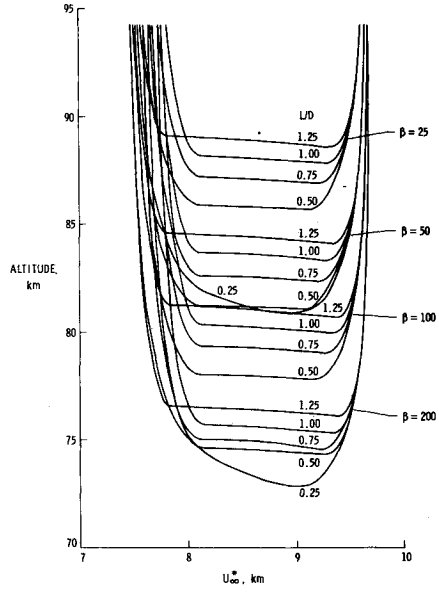

Fig. 1 Near-perigee trajectories for AOTV with various L/D and β.

where $k_{w,i} = k_{wi}^*/U_\infty^*$ is a nondimensionalized recombination rate. The catalytic recombination coefficient (or catalytic efficiency) γ_i is related to $k_{w,i}^*$ by

$$\gamma_i = \sqrt{(2\pi M_i^*/R^*T^*)}\,k_{w,i}^* \tag{2}$$

The total heat transferred to the wall due to conduction and diffusion is

$$q_w = \epsilon^2\left(K\frac{\partial T}{\partial n} + \frac{\mu N_{Le}}{N_{Pr}}\sum_{i=1}^{N_s} h_i\frac{\partial C_i}{\partial n}\right)_w \tag{3}$$

Chemical Kinetics, Thermodynamic, and Transport Properties

The details of the chemical kinetics, thermodynamic, and transport properties used in this study are given in Refs. 8 and 11. Because the enthalpy conditions considered in this study are somewhat higher than in Ref. 8, the thermodynamic properties of each species are extended to higher temperatures with the same method[12,13] of polynomial curve fit applied to the tabulated data of Browne.[14,15]

Method of Solution

Davis[10] presented an implicit finite difference solution to the viscous shock-layer equations for stagnation and downstream flow. Moss[11] applied this method of solution to reacting multicomponent mixtures. The present method of solution is identical to that of Refs. 8 and 11 and, therefore, is not presented.

Limitations of Present Analysis

Although the present method requires much less computing time when compared to the explicit, time-dependent Navier-Stokes solution, it does have some shortcomings. Because those terms higher than second order are dropped from the equation, the solution becomes less accurate as the Reynolds number is decreased. Anderson and Moss[16] have shown that the solution is within 15% of accuracy in the stagnation region at a Reynolds number of 90. Furthermore, the thickening of shock wave for low Reynolds number flow can be approximated only by shock-slip boundary conditions.

Results and Discussion

Laminar convective heating and shock-layer profiles along a representatively blunt body of a 45 deg half-angle hyperboloid with 2.5 m nose radius are presented for a range of acceptable AOTV perigee conditions. The results are obtained from both equilibrium and nonequilibrium viscous shock-layer analyses. The wall temperatures are assumed to be at the radiative equilibrium wall condition with an assumed value of 0.9 for surface emissivity. The nonequilibrium results are calculated using the same dissociative, chemical kinetics that proved[8] to be adequate for predicting the Shuttle flight heating data. However, because of higher enthalpy conditions given for this study, additional investigation including ionization should be considered in the future. For the present nonequilibrium results, the effect of varying surface catalycity, nose radius, half-angle, and vehicle speed on heating reduction are presented, along with comparison of equilibrium and nonequilibrium, equilibrium catalytic wall results.

Freestream Conditions

A family of near-perigee trajectories for AOTV with various values of L/D (0.25-1.25) and β (25-200) are presented in Fig. 1. These trajectories are obtained from the two-dimensional equations of motion with zero inclination angle. To maintain the perigee altitude, the vehicle uses positive or negative lift until the correct velocity decrement has been achieved by drag, then uses lift-up to exit the atmosphere. The degradation of L/D due to high-altitude

viscous effect, as discussed in Ref. 1, has been taken into account in obtaining the trajectories. As can be seen from Fig. 1, the vehicle with the highest value of β and lowest value of L/D has the lowest perigee altitude. It also appears that the value of β has the dominant effect on the perigee altitudes.

For the following results, the 73-90 km perigee altitude and the 8-9.3 km/s vehicle speed as shown in Fig. 1 have been considered. The corresponding freestream quantities, such as density and temperature, have been obtained from the 1976 U.S. Standard Atmosphere.[17]

Effect of Chemistry and Surface Catalycity

The calculated heat-transfer distributions along the body length for the vehicle speed of 8.65 km/s, using both equilibrium and nonequilibrium chemistry are shown in Fig. 2a and 2b for 90 and 77 km altitude, respectively. For the nonequilibrium chemistry, the surface catalytic efficiency γ for both oxygen and nitrogen were varied from 0, 0.01, 0.05, and 0.1 to 1. These constant γ values were chosen strictly for the purpose of a parametric study. (Values of $\gamma = 0.01$ or less are more representative of glassy surfaces at re-entry wall temperatures, while $\gamma = 0.1$ or more would apply to metallic surfaces.) As was expected, the heating distribution increases with increasing γ, but the ratio of increase is quite different for these two altitudes. Moreover, the equilibrium results are higher than the nonequilibrium/equilibrium catalytic wall results by more than 20%. This large difference is not too surprising when one compares the shock-layer profiles for the two types of chemistry used. Figure 3 shows the comparison in temperature, velocity, and species concentration, with an alarmingly large difference in the temperature and atomic nitrogen profile. It should be noted that Figs. 3a and 3b also reveal the existence of a very thick viscous region within the shock layer for all the body locations. The implication of this phenomenon to the choice of analytical methods have been discussed previously.[8]

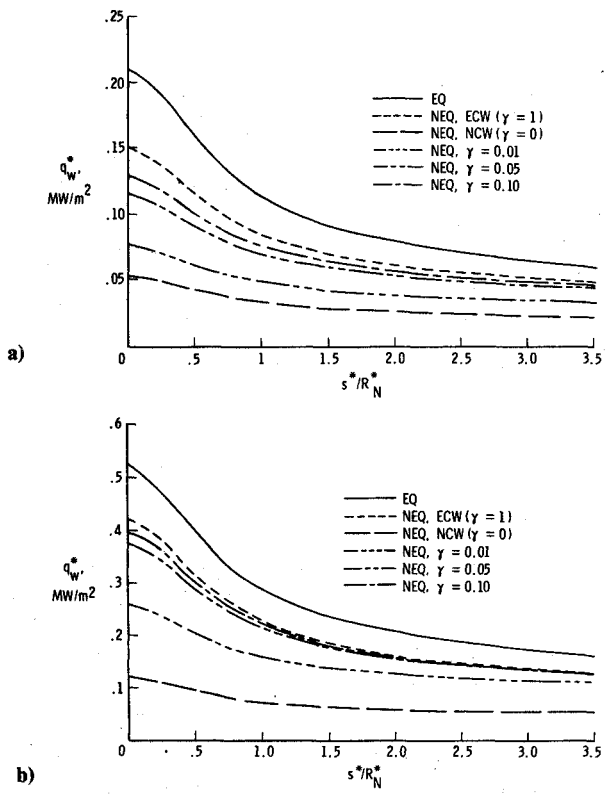

Fig. 2 Heat-transfer distributions on a 45 deg hyperboloid with different chemistry and surface conditions ($R^*_N = 2.5$ m, $U_\infty = 8.65$ km/s): a) altitude = 90 km, b) altitude = 77 km.

It was mentioned earlier that the difference in heating between equilibrium and nonequilibrium, equilibrium catalytic wall results for the vehicle speed of 8.65 km/s is about 20% or more, which is far greater than experienced in the previous[8] Shuttle heating analysis. To examine whether the present higher enthalpy condition is a contributing factor for this large difference, comparison is made for several values of velocity. Figures 4a and 4b show the ratio $q_{w,EQ}/q_{w,\ ECW}$ along the body length for the 77 and 90 km altitudes, respectively. It is evident that as the velocity increases this ratio increases further away from unity. Furthermore, this ratio is greater for the case of 90 km altitude than 77 km, for the reason that the difference in flowfield between these two types of chemistry becomes more severe as the flow becomes more frozen.

Also mentioned earlier, when the surface catalytic efficiency γ is varied, the ratio of increase in heating is quite different for the two different altitudes considered in Fig. 2. Hence, some information for a trend established across the

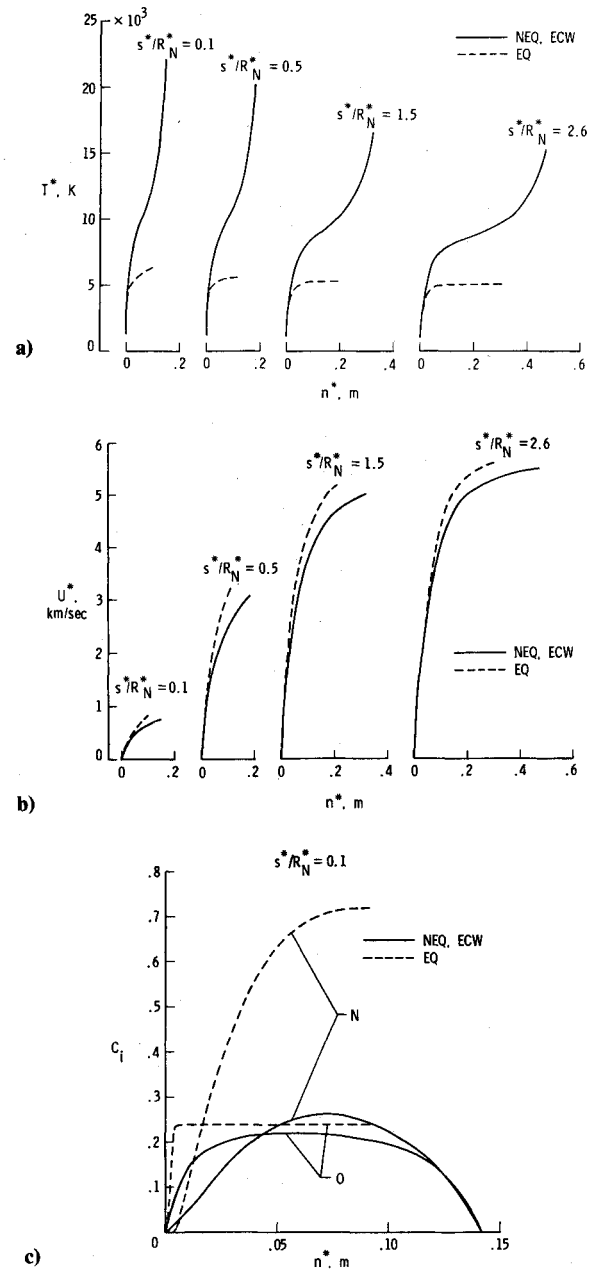

Fig. 3 Shock-layer profile at body locations for a 45 deg hyperboloid ($R^*_N = 2.5$ m, altitude = 90 km, $U^*_\infty = 8.65$ km/s): a) temperature, b) velocity, c) species mass fraction.

altitude range should be desirable for design purposes. Figure 5 shows the heating ratio to the fully catalytic value as a function of altitude for various γ values and body locations. The minimum for $\gamma=0$, which indicates the highest degree of nonequilibrium (at the wall), occurs at an altitude of 81 km. However, as γ increases, the minimum seems to shift away toward a higher altitude. This shifting effect can be explained by the fact that the term $(k_{w,i}\rho N/N_{Le}\mu\epsilon^2)C_i$ in Eq. (1) contains both $k_{w,i}$ and ρ.

To further understand and substantiate the result that the highest degree of nonequilibrium at the wall occurs at an altitude of 81 km, Figs. 6 and 7 are introduced. Figure 6 reveals that the maximum dissociation of nitrogen (at the wall) occurs at the same altitude, with oxygen fully dissociated. Also, the nitrogen mass fraction is shown to exceed the oxygen mass fraction. Hence, with the dissociation energy of nitrogen being almost twice that of oxygen, selection of the thermal protection system (TPS) surface should emphasize the small catalytic efficiency of nitrogen rather than oxygen. Figure 7 illustrates the processes that result in the largest C_N at the wall for 81 km. The temperature profiles in Fig. 7a indicate that the lower the altitude, the faster the temperature decreases from the shock value toward the wall and hence faster dissociation. Figure 7b shows the same trend for the nitrogen dissociation with the lowest altitude of 73 km maintaining the highest nitrogen mass fraction for most of the outer portion of the shock layer. Then, the faster recombination process takes place in the boundary layer for 73 km altitude that results in lower C_N at the wall than for the case of 81 km.

Effect of Configuration Change

The results obtained thus far are for a 45 deg hyperboloid with 2.5 m nose radius. Since the present study is not aimed at a specific OTV configuration, the effect of change in nose radius and half-angle are examined. Figure 8 shows the ratio of noncatalytic heating to the fully catalytic value through the altitude range for 2.5 and 1.25 m nose radii at two body

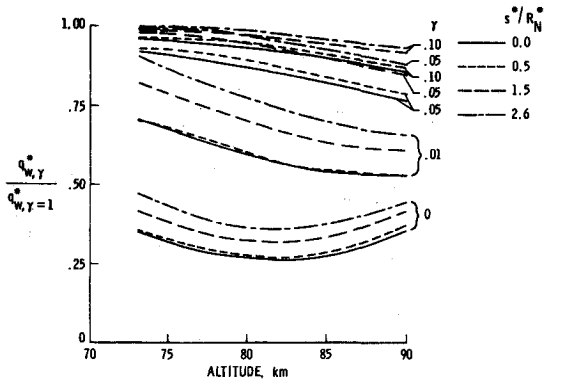

Fig. 5 Ratio of heating to the fully catalytic value as a function of altitude for several γ values and body locations ($R_N^*=2.5$ m, 45 deg hyperboloid, $U_\infty^*=8.65$ km/s).

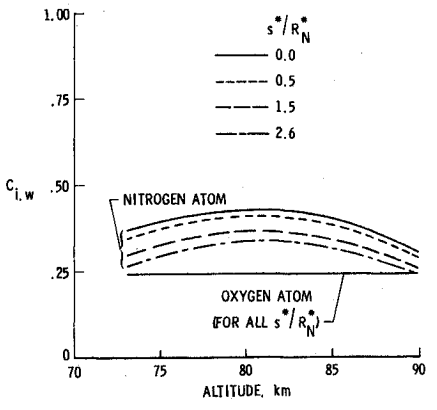

Fig. 6 Atomic species mass fraction at the wall as a function of altitude (noncatalytic wall condition, $R_N^*=2.5$ m, 45 deg hyperboloid, $U_\infty^*=8.65$ km/s).

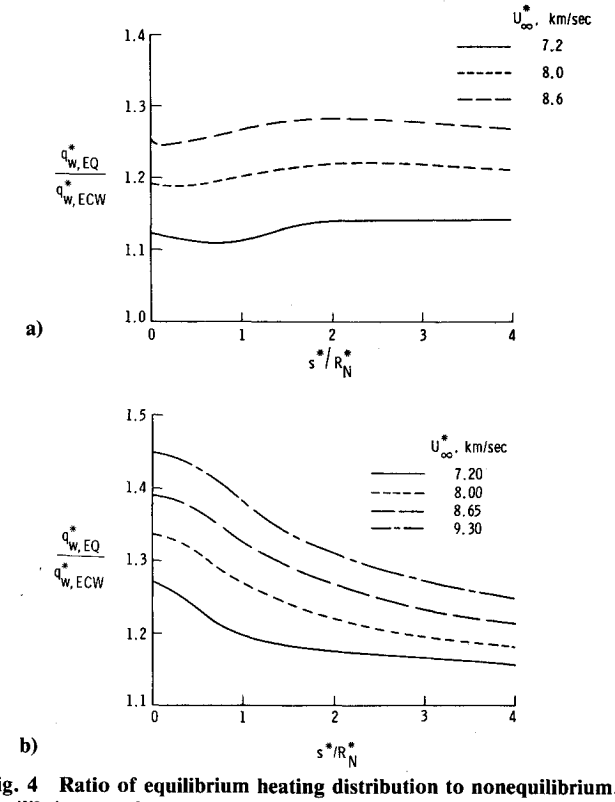

Fig. 4 Ratio of equilibrium heating distribution to nonequilibrium, equilibrium catalytic wall value for different velocities ($R_N^*=2.5$ m, 45 deg hyperboloid): a) altitude = 77 km, b) altitude = 90 km.

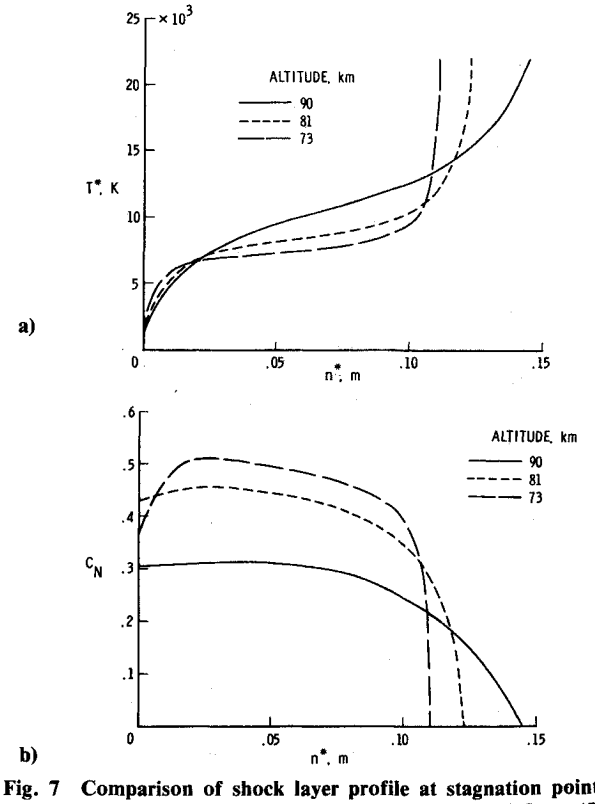

Fig. 7 Comparison of shock layer profile at stagnation point for different altitudes (noncatalytic wall condition, $R_N^*=2.5$ m, 45 deg hyperboloid, $U_\infty^*=8.65$ km/s): a) temperature, b) nitrogen mass fraction.

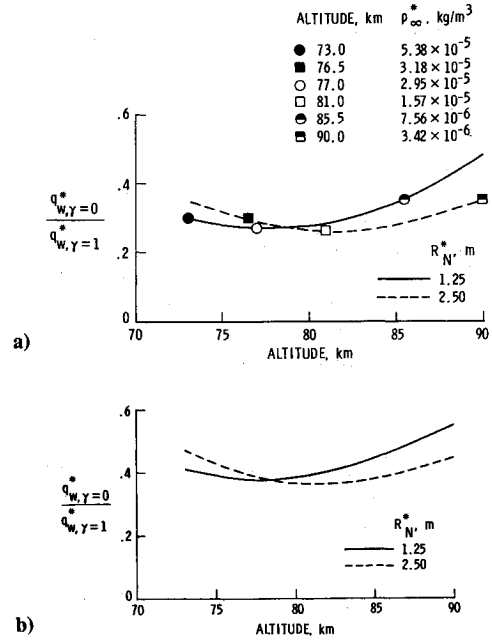

Fig. 8 Effect of nose radius on noncatalytic to fully catalytic heating ratio as a function of altitude (45 deg hyperboloid, $U^*_\infty = 8.65$ km/s): a) $s^*/R^*_N = 0$, b) $s^*/R^*_N = 2.6$.

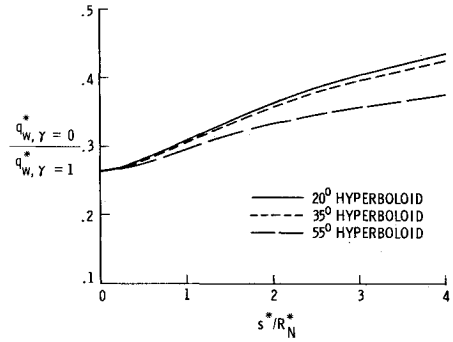

Fig. 9 Effect of body half-angle on noncatalytic to fully catalytic heating ratio distribution ($R^*_N = 2.5$ m, 45 deg hyperboloid, $U^*_\infty = 8.65$ km, altitude = 84 km).

locations. It is seen that, as the nose radius decreases to half, the curve for the heating ratio shift toward a lower altitude, with the minimum of the curve shifting from 81 to 77 km. These two minimums, which are of the same heating ratio, are indicated by an open circle and a square with corresponding tabulated freestream densities in Fig. 8a. It is then immediately clear that as the nose radius is halved, the density is doubled to maintain the same degree of nonequilibrium. Two other examples for the corresponding locations on these two curves are given with a different shade in Fig. 8a. It appears that the product of density and nose radius stays rather constant within each of the three cases, similar to the well-known "binary scaling" law.

It is expected that as the nose radius increases, the minimum of the heating ratio will shift toward higher altitudes. This result should have good implication for using large, high-drag configurations at very high altitudes.

The effect of the varying body half-angle on the nonequilibrium heating reduction along the body length is shown in Fig. 9. The nose radius remained constant, while the body half-angle of the hyperboloid varies from 20 to 55 deg. The results indicate very little or no change in the degree of nonequilibrium for the forebody and about 15% change at a body location of $s^*/R^*_N = 4$.

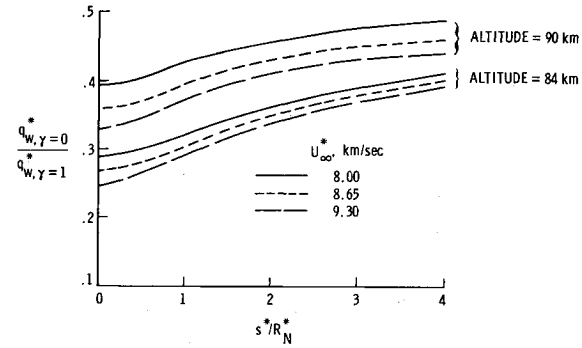

Fig. 10 Effect of velocity on noncatalytic to fully catalytic heating ratio distribution ($R^*_N = 2.5$ m, 45 deg hyperboloid).

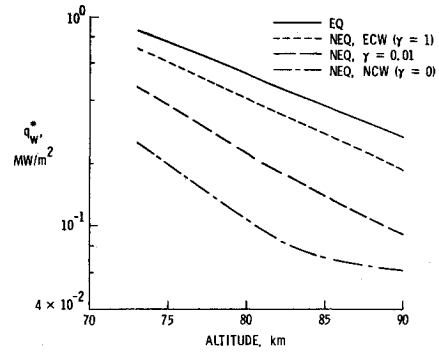

Fig. 11 Maximum perigee heating as a function of altitude for various chemistry and surface conditions ($s^*/R^*_N = 0$, $U^*_\infty = 9.3$ km/s, 45 deg hyperboloid, $R^*_N = 2.5$ m).

Effect of Vehicle Speed

The results obtained thus far for the effect of surface catalycity, nose radius, and half-angle on nonequilibrium heating reduction are for a medium speed of 8.65 km/s. To cover the total spectrum of the perigee conditions in Fig. 1, the effects of varying vehicle speed on nonequilibrium heating reduction are examined. Figure 10 shows the noncatalytic heating ratio to the fully catalytic value along the body length for 84 and 90 km altitude, with the velocity varying 8-9.3 km/s. It is seen that the higher the velocity, the higher the degree of nonequilibrium throughout the body length. Also, it was found earlier that the calculated equilibrium heating becomes much higher than the nonequilibrium, fully catalytic wall result as the velocity increases. Therefore, the ratio of nonequilibrium, noncatalytic heating to the equilibrium value will be even small for higher velocities. The maximum stagnation heating (along the perigee) with different chemistry and surface conditions are shown in Fig. 11 for the altitude range considered in this study.

Conclusion

A parametric study has been obtained for the nonequilibrium flowfield and surface effects on a representatively blunt body, a hyperboloid, at typical AOTV perigee conditions. The results were calculated using a viscous shock-layer code that had previously demonstrated good success in predicting nonequilibrium heating for Shuttle flight data. Several parameters, such as catalytic efficiency, nose radius, and body half-angle were varied and the following conclusions are obtained:

1) Due to higher velocity for AOTV than Space Shuttle, the flowfield for AOTV's are of higher degree of nonequilibrium with substantial nitrogen dissociation. Hence, the selection of a TPS surface with small nitrogen recombination rate will be more beneficial than a selection based on the oxygen rate.

Furthermore, the equilibrium heating results are much higher than the nonequilibrium, fully catalytic results.

2) The highest degree of nonequilibrium is found at 81 km for 2.5 m nose radius; however, as the surface becomes slightly catalytic, the largest heating reduction shifts toward higher altitude.

3) When the nose radius varies, the altitude at which the same degree of nonequilibrium occurs changes accordingly, so that the product of density and nose radius remain almost constant. This result should have good implication for using a large, high-drag configuration at very high altitude.

4) As the half-angle varies between 20-55 deg, little change in nonequilibrium heating reduction is observed.

Although the present study for AOTV uses the same dissociation chemistry as in the previous Shuttle analysis, future investigation including ionization should be considered.

References

[1]Walberg, G.D., "A Review of Aeroassisted Orbit Transfer." AIAA Paper 82-1378, Aug. 1982.

[2]Ketter, F.C. Jr., "Results of Tests to Determine the Aerodynamic Characteristics of Two Potential Aeromaneuvering Orbit-to-Orbit Shuttle (AMOOS) Vehicle Configurations in the NASA Ames 3.5-Foot Hypersonic Wind Tunnel," Lockheed Missiles and Space Co., Huntsville, Ala., NASA CR-120423, May 1974.

[3]White, J., "Feasibility and Tradeoff Study of an Aeromaneuvering Orbit-to-Orbit Shuttle (AMOOS)," Lockheed Missiles and Space Co., Huntsville, Ala., NASA CR-130431, July 1974.

[4]Hethcoat, J.P., "Aeromaneuvering Orbit Transfer Vehicles for the Space Transport System," IAF Paper 76-173, Oct. 1976.

[5]Heald, D.A., "Is a Versatile Orbit Transfer Stage Feasible—Orbit Transfer Concepts, Potential Missions and Evolution," AIAA Paper 79-0866, May 1979.

[6]Grenich, A.F. and Woods, W.C., "Flow Field Investigation of Atmospheric Braking for High Drag Vehicles with Forward Facing Jets in Spacecraft Entry," AIAA Paper 81-0293, Jan. 1981.

[7]Andrews, D.G. and Bloetscher, F., "Aerobraked Orbital Transfer Vehicle Definition," AIAA Paper 81-0279, Jan. 1981.

[8]Shinn, J.L., Moss, J.N., and Simmonds, A.L., "Viscous Shock-Layer Heating Analysis for the Shuttle Windward-Symmetry Plane with Surface Finite Catalytic Recombination Rates," AIAA Paper 82-0842, June 1982, also *AIAA Progress in Astronautics and Aeronautics*, Vol. 85, edited by Bauer and Collicott, 1983, pp. 149-180.

[9]Austin, R.C., Cruz, M.I., and French, J.R., "System Design Concepts and Requirements for Aeroassisted Orbital Transfer Vehicles," AIAA Paper 82-1379, Aug. 1982.

[10]Davis, R.T., "Numerical Solution of the Hypersonic Viscous Shock-Layer Equations," *AIAA Journal*, Vol. 8, May 1970, pp. 843-851.

[11]Moss, James N., "Reacting Viscous-Shock-Layer Solutions with Multicomponent Diffusion and Mass Injection," NASA TR R-411, 1974.

[12]Esch, D.D., Siripong, A., and Pike, R.W., "Thermodynamic Properties in Polynomial Form for Carbon, Hydrogen, and Oxygen Systems from 300 to 15,000° K," NASA CR-111989, 1970.

[13]Gordon, S. and McBride, B.J., "Computer Program for Calculation of Complex Chemical Equilibrium Compositions, Rocket Performance, Incident and Reflected Shocks, and Chapman-Jouguet Detonations," NASA SP-273, 1971.

[14]Browne, W.G., "Thermodynamic Properties of Some Atoms and Atomic Ions," General Electric Co., MSVD Engineering Physics Tech. Memo. 2, 1962.

[15]Browne, W.G., "Thermodynamic Properties of Some Diatoms and Diatomic Ions," General Electric Co., MSVD Engineering Physics Tech. Memo. 8, May 14, 1982.

[16]Anderson, E.C. and Moss, James N., "Numerical Solution of the Steady-State Navier-Stokes Equations for Hypersonic Flow About Blunt Axisymmetric Bodies," NASA TM X-71977, June 1974.

[17]*U.S. Standard Atmosphere, 1976*, NOAA, NASA, and U.S. Air Force, Oct. 1976.